Aortic Shape Space Topology

Kameel Khabaz[1*], Seth Sankary[1], Karen Yuan[1], Joseph Pugar[2], Sanjeev Dhara[1], Junsung Kim[1], Janet Kang[1], Nhung Nguyen[1], Kathleen Cao[1], Nicole Pierce[1], CJ Lee[3], Ross Milner[1], Gordon Kindlmann[4] and Luka Pocivavsek[1]

[1]Department of Surgery, The University of Chicago, 5841 S. Maryland Drive, Chicago, 60637, IL, USA.
[2]Department of Material Science, Carnegie Mellon University, Shadyside, Pittsburgh, 15212, PA, USA.
[3]Department of Surgery, NorthShore University Healthcare System, Case Drive, Evanston, 60637, IL, USA.
[4]Department of Computer Science, The University of Chicago, 5730 S. Ellis Ave., Chicago, 60637, IL, USA.

Contributing authors: lpociavsek@bsd.uchicago.edu;

Abstract

Cross-sectional imaging, such as computed tomography (CTA) scans, provide unparalleled visualization of aortic anatomy. However, despite the immense geometric and anatomic detail provided by CTA imaging, surgeons continue to interact with this data in a linear and dimensionally reduced feature space. Aortic pathologies such as aneurysms and dissections are clinically quantified using a single scalar: maximum aortic diameter. To date, not feature of aortic shape has reproducibly captured what surgeons often describe qualitatively when looking at CT scans or when in the operating room observing the physical anatomy. Shape along with size plays a central role in differentiating normal from diseased aortas. We defined a geometric feature space using tools of modern differential geometry that incorporate shape and size. We show that size can be parameterized by $\boldsymbol{\ell}$, the radial aortic extent commonly taken as aortic diameter. Size invariant shape is quantified by performing a Gauss map of local regions on the aortic surface and calculating the variance of the total integrated curvature ($\boldsymbol{\delta K}$) across each aorta. While we do not inherently study aortic stability as it relates to clinical rupture in this paper, aortas appearing at high $\boldsymbol{\delta K}$ are clinically classified by size and qualitative appearance as high risk. It is therefor interesting to conjecture that divergence in the $(\boldsymbol{\delta K}, \tilde{\boldsymbol{\ell}})$-space is a sign of aortic topologic instability. Projection into $(\boldsymbol{\delta K}, \tilde{\boldsymbol{\ell}})$-space provides two independent variables that show a natural division of the data as it transitions from size to shape dominated behavior, an indictor of aortic fragility.

Keywords: aorta, topology, shape, classification

The problem of morphogensis is deeply linked to the stability of growing structures; René Thom postulated that the precise mathematical form of any morphological process is defined by topologic homeomorphisms [2, 3, 66]. Topology is now a fundamental tool in the classification of rapidly changing shapes and structures in developmental biology [4]. This paper is a novel application of topology in aortic morphogenesis. Aortic rupture almost inevitably leads to death; as such, the paradigm of aortic clinical management is

preventative surgery [32–35]. As the up-front risk of surgery decreases while the risk of long-term repair failure increases with endovascular approaches, critical gaps in knowledge are appearing in patient selection for aortic operations [6, 29, 35, 37, 62, 63], placing increasing pressure on defining an appropriate classification space for aortic fragility.

Figure 1 shows eight representative aortic shapes spread along the normal-to-pathologic axis of aortic morphology. Qualitatively, the aortas to the right become bumpy and torturous in space, breaking the smoothness of the toroidal-cylindrical symmetry. Descriptors of diseased thoracic aortas used by pioneers of aortic surgery such as Michael DeBakey include: 'torturous', 'globular', 'U-shaped', 'dilated', and 'idiosyncratically varying' [32–34], terms often repeated by surgeons today. The open challenge of aortic morphogenesis is independent parameters for quantifying size and shape, mathematical descriptors of what the clinician visually describes with ease. A longstanding clinically-standard parameterization of size is based on the maximum aortic diameter, $2R_m$, [7, 28, 35]. In the first part of this paper, we show that all measures of aortic size collapse onto a linear master scaling curve, indicating that there is no additional information to be had by higher-order functions of size, such as aortic surface area (A_T) or volume (V), motivating the study of shape in the second half of this paper.

Segmentations are surface representations of the aortic wall derived from contrast enhanced computed tomography scans; three-hundred and two aortic segmentations (spanning from a healthy 3-year old child to an aneurysmal type B aortic dissection in an 92-year old) are converted to triangulated meshed surfaces containing geometric information about each aorta (see Methods). Visual inspection of the aortas in Figure 1 leads to the hypothesis that any aorta is globally a generalized bent cylinder parameterized by two length scales: cross-sectional extent ℓ and axial length $\mathcal{L}$. While R_m is clinically dominant, other lengths can define ℓ including: mean aortic radius ($\langle R \rangle$), median aortic radius ($\widetilde{R_2}$), and the mean inverse linearized aortic Casorati curvature, $\langle C^{1/2} \rangle^{-1}$. $C_i^{1/2}$ is the Frobenious norm of $\mathbb{S}_i$, the per-vertex aortic shape operator (see figure 1) [46–49]. In Figure 2 Ia., we plot each one of these measures of ℓ versus $\widetilde{R_2}$; the data all collapse onto lines with slope 1, proving the equivalency of the different length scales. We also plot the square root and cube root of total aortic area and volume, respectively. Remarkably, these scalings also collapse onto lines, proving that globally all aortas are generalized cylinders with aortic area and volume scaling as $A_T \sim 2\pi c \ell^2$ and $V \sim \pi c \ell^3$, where we used the reparameterization $\mathcal{L} \sim c\ell$. The proportionality constant $c \sim 15$ can be obtained from the linear fits and independently verified by defining $\mathcal{L}$ as the centerline length of each segmentation and inverting the reparameterization.

Normalization with the above pre-factors collapses all of the size measures onto a single master line (see Figure 2 Ib.); as such, irrespective of how much aortic surfaces distort from one person to another by growing, stretching, twisting, or bending they globally retain a generalized cylindrical geometry concerning their overall area and volume. Furthermore, because of this invariant global geometry, the parametrization of size is dependent only on the single length scale ℓ. The clinical literature is increasingly focused on using direct measurement of A_T or V to quantify size with the intent of discovering additional information for aortic classification presumedly lost with simply measuring ℓ [15–19]. Our analysis shows additional information is unlikely to exist with such global higher dimensional measurements, and provides the quantitative basis behind the incredible utility of maximum diameter throughout the decades of aortic management [29].

Clinically, the need for a mathematical definition of aortic shape is driven by the known problems of using size alone in decision making for various aortic pathologies including coarctations [20], aneurysms [51–60, 63, 64], and aortic dissections [21–26]. Specific extrinsic measures of aortic shape have focused on functions of mean, $\kappa_m = (k_1 + k_2)/2$, or Gaussian curvature, $\kappa_g = k_1 k_2$, [52–56], deviation of aortic cross-section from a circle termed eccentricity [25, 26], and a very large literature of calculations on Elastica-like reductions of the aortic surface to a space curve, termed the centerline in clinical literature, leading to measures of curve tortuosity [21–24], mean curvature [67], and bending [27]. Two problems exists in the current methods: spatial over reduction and convolution of shape/size information. Normalized centerline calculations obtain shape only information, however reducing the highly heterogeneous aortic surfaces to a space curve causes the loss of large amounts of shape information. κ_g contains shape information that is convoluted with size, since κ_g is not a dimensionless quantity [38, 40]. We seek a surface based function that measures shape across all aortic sizes.

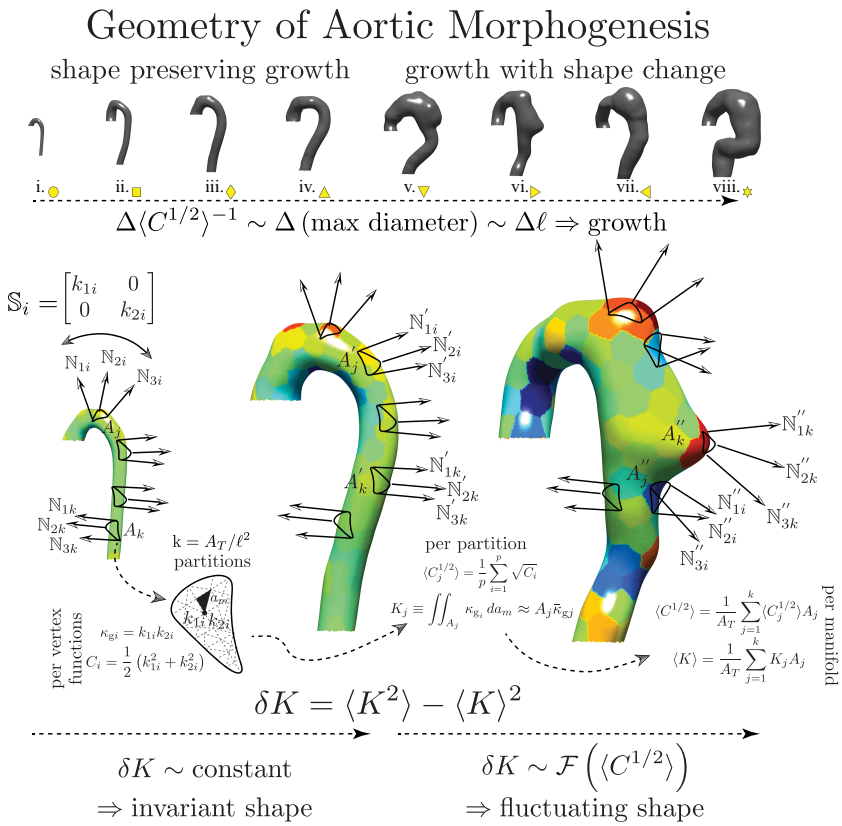

Fig. 1 Top panel shows a representative set of aortic segmentation geometries from computed tomography scans: i. through iii. are normal non-diseased aortas ranging from a 3 year-old child (i.) to healthy adults (ii. and iii.); iv. through viii. are type B aortic dissection (TBAD) patients at varying degrees of aneurysmal degeneration. Visual inspection of the representative aortic geometries shows that two regimes exist: shape preserving growth and growth with shape changes; the former occurring during normal development and the later during pathology. The problem is to identify a parameter space where this visual observation can be quantitated. Aortic geometry is characterized by two parameters: size and shape. The per-vertex aortic shape operator $\mathbb{S}_i$ contains complete information on both size and shape. Traditional invariants of $\mathbb{S}_i$, mean and Gaussian curvatures, convolute shape and size, as do many published geometric classifiers, see supplemental figure 3b and 5. The Casorati curvature, C_i, and the total curvature, K_j, are orthogonal functions of $\mathbb{S}_i$ and provide independent information on size and shape, respectively. $\mathbb{S}_i$ is the diagonalized spatial gradient of surface normals calculated on a generic computational mesh placed on the aortic segmentations [40, 41]. The squared Frobenius norm of $\mathbb{S}_i$ gives C_i [46, 47, 49]. Information about shape is embedded in the per vertex Gaussian curvature, κ_{gi}. By integrating κ_{gi} over a given surface area, we remove the size dependence and are left with a shape-dominated function, the total curvature: $K_j = \iint_{A_j} \kappa_{g_i} da_m \approx A_j\bar{\kappa}_{gj}$. Key in our analysis is developing a consistent self-contained method for defining A_j, the area over which the integral is taken; this method must scale across all aortic shapes and sizes. A single universal length scale ℓ contains all the information on size, despite various methods of measuring it (see figure 2I). We use ℓ to divide the surface into k partitions, $k = A_T\ell^{-2}$; defined this way, the number of partitions is $O(100)$ and constant over many shapes and sizes (see figure 2Ic). Per partition K_j and $\langle C_j^{1/2}\rangle$ are computed and then averaged over the entire aorta to give the per manifold scalar values $\langle K\rangle$ and $\langle C^{1/2}\rangle$. These two functions are orthogonal to each other and contain independent information about aortic size and shape. The breakdown of normal versus pathologic aortic shape is linked to the fluctuations in total aortic curvature, defined as $\delta K = \langle K^2\rangle - \langle K\rangle^2$. This allows a mathematical formalism in which to quantitatively classify aortas into a regime of self-similar shape invariant growth, $\delta K \sim$ constant, and a symmetry-breaking regime where shape fluctuations diverge with a given functional dependence on mean size, $\delta K \sim \mathcal{F}\left(\langle C^{1/2}\rangle\right)$.

The Gauss map defines a normalized space where all surface shapes can be compared irrespective of their size by mapping the aortic surface $\mathcal{S}$ to a unit sphere $\mathbf{S}^2$ [38, 40]. Figure 1 outlines our computational methodology where we implement the Gauss map by calculating the total curvature: $K = \iint_A \kappa_g dA$

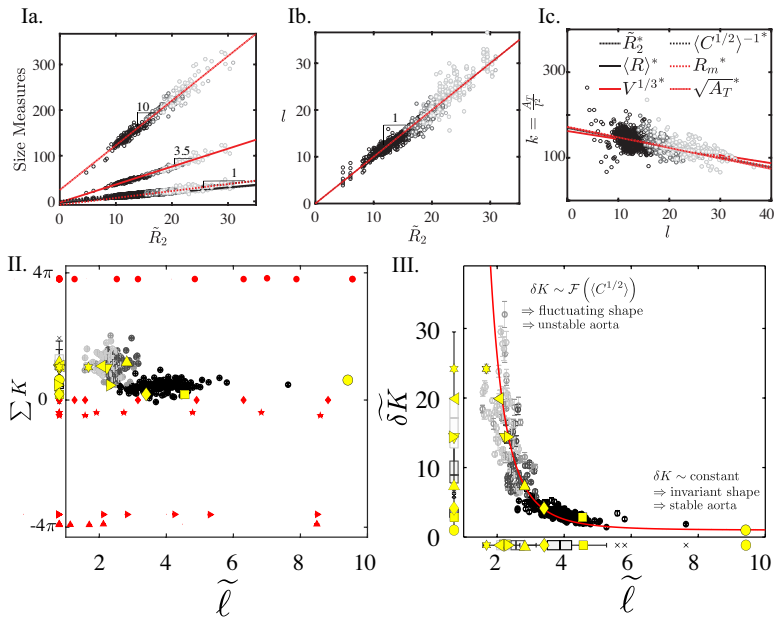

Fig. 2 **Ia.** A vast distribution of aortas shows that there is a completely linear scaling between $\widetilde{R}$ and different measures of aortic size, when appropriately dimensionalized: total aortic area A_T, aortic volume V, mean aortic radius $\langle R \rangle$, maximum aortic radius R_m, median aortic radius calculated from the second principal curvature $\widetilde{R_2}$, and the dimensionalized mean of the inverse Casorati curvature $\langle C^{1/2} \rangle^{-1}$. The single length measures of size exhibit linear equivalence with $\widetilde{R}$ with a pre-factor of $O(1)$. We see that $A_T \approx 10\widetilde{R}$ and $V \approx 3.5\widetilde{R}$. When assuming a cylindrical geometry, $A_T \sim 2\pi\widetilde{R} \times \mathcal{L}$ and $V \sim \pi\widetilde{R}^2 \times \mathcal{L}$ and an anatomic scaling between length and width $\mathcal{L} \sim c\widetilde{R}$, we get $c \sim 15$. This approximation if validated by measuring $c \sim L/\langle C^{1/2} \rangle^{-1}$, where L is the length of the aortic centerline (Supplemental Figure x). **Ib.** The size measures are collapsed onto the same master line, demonstrating that there is little extra information that can be gained by measuring global areas or volumes to characterize aortic size, a before unappreciated observation in the aortic clinical literature. **Ic.** Calculation of k using different size measures, after collapsed onto the master curve, returns similar results. **II.** The total curvature $\sum K$ is approximately constant among aortas of vastly differing shapes and sizes, demonstrating that $\sum K$ is a topologic invariant. II: The patients are plotted as in part III of the figure (see below). Circles are depicted as spheres. Tori are depicted as stars. Cylinders are depicted as diamonds. Pseudospheres are depicted as rightward-pointing triangles. Catenoids are depicted by upward-pointing triangles. **III.**: δK versus $\tilde{\ell}$. Different patient cohorts are shown in grayscale Black (0/1 grayscale) indicates non-pathologic aortas. Dark gray (0.3/1 grayscale) indicates the final pre-operative and all post-operative scans for the desired outcomes TBAD cohort. Light gray (0.8/1 grayscale) indicates the final pre-operative and all post-operative scans for the failed outcomes TBAD cohort. The data with intermediate grayscale (0.6/1) represents either pre-operative scans (excluding the final pre-op scan) or the non-TBAD aortic disease scans. The yellow shapes are data for the progression panel in Figure 1. The data fit onto a universal scaling law given by $\widetilde{\delta K} = (4.5\tilde{\ell})^4 + 1$.

(see Methods for details). To calculate K using extrinsic geometry of the highly heterogenous aortic surfaces, A_T is subdivided into k partitions each with area A_j. Enforcing weak κ_g spatial variation by minimizing the Jensen-Shannon divergence of κ_g within each partition (see supplemental figure S3), the upper limit of A_j is set. This allows the per partition mean $\bar{\kappa}_{gj}$ to be treated as constant and taken outside the integral for K. The lower limit on A_j is set by the discretization of the surface; each element with area a_{mi} is locally Euclidean; on a curved portion of the surface, A_j must be large enough such that $\sum_i^p a_{mi}$ captures the correct area scaling [43, 44]. The local per partition total curvature becomes $K_j = A_j\bar{\kappa}_{gj}$. In our analysis, A_j can vary by $O(10)$ and not impact the data (see supplemental figure S4). Figure 2 II plots $\sum K$ as a function of normalized size $\tilde{\ell} = \ell/\sqrt{A_{T,min}}$. All aortas fall on a line just above $K = 0$ (horizontal fit to data intercepts y-axis at $\frac{2}{3}\pi$) proving the topologic invariance of aortic shapes and their homeomorphism to $\mathbf{T}^2 = S^1 \times S^1 + S^1 \times \mathbf{R} = \mathbf{T}^2$. Topology preservation is by far not the norm in biologically growing surfaces that are non-conservative and can locally add mass or remove mass without the constraint of elastic deformations or linkage to some global manifold [66]. The discovery of a topologic isomorphism in aortic morphogenesis allows the conjecture that a global mechanical field strongly couples to aortic shape even in highly diseased aortic states [2, 3, 3, 66].

The existence of a homeomorphism further implies that as aortas deform be it through normal growth or pathology every increase in K in some

region must be balanced by a proportional decrease somewhere else on the aortic surface [70]. Therefore, the distribution of K across the aortic surface holds information about shape. This allows us to classify shape by studying the statistical properties of these distributions. Since $\langle K \rangle$ is constant the variance of K captures the balance of positive and negative curvature regions across the surface: $\delta K = \langle K^2 \rangle - \langle K \rangle^2$. Figure 2 III. plots δK as a function of normalized size. Normal aortas (black circles) have a nearly constant δK from the smallest aorta in a 3-year old child to the largest in a 92-year old. $\delta K \sim$ constant is thus the mathematical signature of shape preserving growth seen in normal aortas. As pathology develops (primarily in the form of aneurysmal degeneration following aortic dissection) δK rapidly increases. Two populations of diseased patients are shown in the figure: dark grey circles correspond to patients who underwent successful aortic repair with endovascular stent graft placement (TEVAR) while the lighter gray data, at even higher δK values, are patients where TEVAR ultimately failed as a treatment. As such, rapidly increasing δK is a clear signature of aortic degeneration, corresponding to a highly fluctuating shape different from the smooth toroidal-cylinder. The data projected in the $(\delta K, \tilde{\ell})$-space can be fit to a power law $\widetilde{\delta K} = (4.5\tilde{\ell})^4 + 1$. The existence of a power law behavior is further supported by the power-law probability distribution of δK (see supplemental figure S7).

No general theory exists on the meaning of δK divergence. However in soft matter systems such as spherical vesicles, where size weakly changes, and in dynamical systems rapid fluctuations of κ_g have been linked to so-called 'topologic catastrophes' indicative of approaching instabilities. In vesicles, the instability manifests as the physical breakup of the system: budding, fusion, or rupture; in dynamic systems, the topologic catastrophe indicates the development of trubulence. While we do not inherently study aortic stability as it relates to clinical rupture in this paper, aortas appearing at high δK are clinically classified by size and qualitative appearance as high risk. It is therefor interesting to conjecture that divergence in the $(\delta K, \tilde{\ell})$-space is a sign of aortic topologic instability and an indicator of aortic fragility.

To further study δK as an aortic descriptor, machine learning (ML) methods were used to quantify its utility as a patient classification feature among other shape measurements. As mentioned above, our cohort includes two diseased patient populations which are classified based upon their clinical outcomes with TEVAR. ML can be used to build predictive classification models from sets of training data by identifying and leveraging underlying trends to make predictions and thus can be built to predict outcomes from size and shape measurements. Using a logistic regression model, we show that δK significantly outperforms all available measures of shape (Figure S13 Ib. and Table S3) both in the 2-class (intra-group separation within the diseased aortas) and the 3-class (including normal aortas) problem. This result can be interpreted as δK being the best second parameter to add to ℓ in creating a two dimensional shape$\times$size space from which the most accurate classification occurs. The analysis also shows statistical parity between all measures of size (Figure S13 Ib.) independently validating our geometric analysis in Figure 2. Furthermore, a single variable linear space defined by maximum diameter, while widely used, is inherently problematic because a critical point between closely spaced and overlapping normally distributed populations is very sensitive to the available data (Figure S14 I.); a well-known problem in maximum diameter based criteria is the bias against smaller statured female patients because of the heavily male-waited population-based statistics on aortic sizes [68, 69]. Projection into $(\delta K, \tilde{\ell})$-space provides two independent variables that show a natural division of the data as it transitions from size to shape dominated behavior as seen in Figure S14 II. 2-class and 3-class classification is significantly more accurate in the $(\delta K, \tilde{\ell})$-space compared to the R_m-space, moreover the former is far more robust and less sensitive to data variability. Lastly, while the ML model's learned decision boundaries (i.e., classification thresholds) are limited in their universal interpretation, they do offer an unbiased source of evidence that 1. Introducing δK improves class separation and classification accuracy most among other shape factors and 2. An underlying transition between successful and failed TEVAR may be primarily governed by aortic shape factors.

Acknowledgments: We acknowledge the support of the National Institutes of Health, NHLBI, R01HL159205.

References

[1] R. Thome. *Topological Models in Biology.* Topology. 1969; 8:313-335.

[2] Maresin, V.M. and Presnov, E. *Topological Approach to Embryogenesis.* J. Theor. Biol. 1985; 114:387-398.

[3] Presnov, E., V, Isaeva, and N. Kasyanov. *Topological Invariance of Biological Development.* Axiomathes. 2014; 24:117-134.

[4] Jockusch, H. and A. Dress. *From Sphere to Torus: A Topological View of the Metazoan Body Plan.* Bulletin of Mathematical Topology. 2002; 65:57-65.

[5] Yuan X, Clough RE, Nienaber CA. *Management of Uncomplicated Type B Aortic Dissection.* Hearts. 2020;1(1):14-24. doi:10.3390/hearts1010004

[6] Tsai TT, Trimarchi S, Nienaber CA. *Acute Aortic Dissection: Perspectives from the International Registry of Acute Aortic Dissection (IRAD).* Eur J Vasc Endovasc Surg. 2009;37(2):149-159. doi:10.1016/j.ejvs.2008.11.032

[7] Nauta FJ, Trimarchi S, Kamman AV, et al. *Update in the management of type B aortic dissection.* Vasc Med. 2016;21(3):251-263. doi:10.1177/1358863X16642318

[8] Moulakakis KG, Mylonas SN, Dalainas I, Kakisis J, Kotsis T, Liapis CD. *Management of complicated and uncomplicated acute type B dissection. A systematic review and meta-analysis.* Ann Cardiothorac Surg. 2014;3(3):13.

[9] Luebke T, Brunkwall J. *Type B Aortic Dissection: A Review of Prognostic Factors and Meta-analysis of Treatment Options Based on a Presentation at the 2013 VEITH Symposium, November 1923, 2013 (New York, NY, USA).* AORTA J. 2014;2(6):265-278. doi:10.12945/j.aorta.2014.14-040.

[10] Fattori R, Montgomery D, Lovato L, et al. *Survival After Endovascular Therapy in Patients With Type B Aortic Dissection: A Report From the International Registry of Acute Aortic Dissection (IRAD).* JACC Cardiovasc Interv. 2013;6(8):876-882. doi:10.1016/j.jcin.2013.05.003

[11] Stanley GA, Murphy EH, Knowles M, et al. *Volumetric analysis of type B aortic dissections treated with thoracic endovascular aortic repair.* J Vasc Surg. 2011;54(4):985-992. doi:10.1016/j.jvs.2011.03.263

[12] Nienaber CA, Kische S, Rousseau H, et al. *Endovascular Repair of Type B Aortic Dissection.* Circ Cardiovasc Interv. 2013;6(4):407-416. doi:10.1161/CIRCINTERVENTIONS.113.000463

[13] Enezate TH, Omran J, Al-Dadah AS, et al. *Thoracic endovascular repair versus medical management for acute uncomplicated type B aortic dissection.* Catheter Cardiovasc Interv Off J Soc Card Angiogr Interv. 2018;91(6):1138-1143. doi:10.1002/ccd.27406

[14] Nienaber CA, Rousseau H, Eggebrecht H, et al. *Randomized comparison of strategies for type B aortic dissection: the INvestigation of STEnt Grafts in Aortic Dissection (INSTEAD) trial.* Circulation. 2009;120(25):2519-2528. doi:10.1161/CIRCULATIONAHA.109.886408

[15] Qin YL, Deng G, Li TX, Jing RW, Teng GJ. *Risk factors of incomplete thrombosis in the false lumen after endovascular treatment of extensive acute type B aortic dissection.* J Vasc Surg. 2012;56(5):1232-1238. doi:10.1016/j.jvs.2012.04.019

[16] Song JM, Kim SD, Kim JH, et al. *Long-Term Predictors of Descending Aorta Aneurysmal Change in Patients With Aortic Dissection.* J Am Coll Cardiol. 2007;50(8):799-804. doi:10.1016/j.jacc.2007.03.064

[17] Immer FF, Krahenbuhl E, Hagen U, et al. *Large Area of the False Lumen Favors Secondary Dilatation of the Aorta After Acute Type A Aortic Dissection.* Circulation. 2005; 112 (9 supplement): I-249. I-249. doi:10.1161/ CIRCULATIONAHA.104.525733

[18] Kim TH, Ko YG, Woo Kwon S, et al. *Large False Lumen Area Is a Predictor of*

Failed False Lumen Volume Reduction After Stent-Graft Repair in Type B Aortic Dissection. J Endovasc Ther. 2014;21(5):697-706. doi:10.1583/14-4671MR.1

[19] Chang CP, Liu JC, Liou YM, Chang SS, Chen JY. *The Role of False Lumen Size in Prediction of In-Hospital Complications After Acute Type B Aortic Dissection.* J Am Coll Cardiol. 2008;52(14):1170-1176. doi:10.1016/j.jacc.2008.06.034

[20] Bruse JL, Khushnood A, McLeod K, et al. *How successful is successful? Aortic arch shape after successful aortic coarctation repair correlates with left ventricular function.* J Thorac Cardiovasc Surg. 2017;153(2):418-427. doi:10.1016/j.jtcvs.2016.09.018

[21] Chen CK, Liang IP, Chang HT, et al. *Impact on outcomes by measuring tortuosity with reporting standards for thoracic endovascular aortic repair.* J Vasc Surg. 2014;60(4):937-944. doi:10.1016/j.jvs.2014.04.008

[22] Ueda T, Takaoka H, Raman B, Rosenberg J, Rubin G. *Impact of Quantitatively Determined Native Thoracic Aortic Tortuosity on Endoleak Development After Thoracic Endovascular Aortic Repair.* AJR Am J Roentgenol. 2011;197:W1140-6. doi:10.2214/AJR.11.6819

[23] Boufi M, Guivier-Curien C, Dona B, et al. *Risk Factor Analysis for the Mal-Positioning of Thoracic Aortic Stent Grafts.* Eur J Vasc Endovasc Surg. 2016;52(1):56-63. doi:10.1016/j.ejvs.2016.03.025

[24] Bowman JN, Silverberg D, Ellozy S, et al. *The Role of Anatomic Factors in Predicting Success of Endovascular Repair of Thoracic Aortic Aneurysms.* Vasc Endovascular Surg. 2010;44(2):101-104. doi:10.1177/1538574409347392

[25] Suh GY, Bondesson J, Zhu YD, Lee JT, Dake MD, Cheng CP. *Multiaxial pulsatile dynamics of the thoracic aorta and impact of thoracic endovascular repair.* Eur J Radiol Open. 2021;8:100333. doi:10.1016/j.ejro.2021.100333

[26] Bondesson J, Suh GY, Marks N, Dake MD, Lee JT, Cheng CP. *Influence of thoracic endovascular aortic repair on true lumen helical morphology for Stanford type B dissections.* J Vasc Surg. 2021;74(5):1499-1507.e1. doi:10.1016/j.jvs.2021.04.029

[27] Li D, Peng L, Wang Y, Zhao J, Yuan D, Zheng T. *Predictor of false lumen thrombosis after thoracic endovascular aortic repair for type B dissection.* J Thorac Cardiovasc Surg. 2020;160(2):360-367. doi:10.1016/j.jtcvs.2019.07.091

[28] Paruchuri V, Salhab KF, Kuzmik G, et al. *Aortic Size Distribution in the General Population: Explaining the Size Paradox in Aortic Dissection.* Cardiology. 2015;131(4):265-272. doi:10.1159/000381281

[29] Spinelli, D., F. Benedetto, R. Donato, G. Piffaretti, M.M. Marrocco-Trischitta, H.J. Patel, K.A. Eagle, and S. Trimarchi. *Current Evidence in the Predictors of Aortic Growth and Events in Acute Type B Aortic Dissection.* J. Vasc. Surg. 2018; 68: 1925-1935.

[30] M.A. Coady, J.A. Rizzo, G.L. Hammond, D. Mandapati, U. Darr, G.S. Kopf, and J.A. Elefteriades *What is the Appropriate Size Criterion for Resection of Thoracic Aortic Aneurysms?.* J. Thorac. Cardiovasc. Surg. 1997; 113: 476-491.

[31] S.A. Goldstein et al. *Multimodality Imaging of Disease of the Thoracic Aorta in Adults: from the American Society of Echocardiography and the European Association of Cardiovascular Imaging.* J. Am. Soc. Echocardiogr. 2015; 28: 119-182.

[32] DeBakey, M.E. and D.A. Cooley, *Successful Resection of Aneurysm of Thoracic Aorta and Replacement by Graft* J.A.M.A., 1953. **152** (8): p. 673-676.

[33] DeBakey, M.E., D.A. Cooley, and O. Creech, *Surgical Considerations of Dissecting Aneurysm of the Aorta* Annals of Surgery, 1955. **142** (4): p. 586-610.

[34] Dake, M.D., D.C. Milber, C.P. Semba, R.S. Mitchell, P.J. Walker, and R.P. Liddell. *Transluminal Placement of Endovascular Stent-Grafts for the Treatment of Descending Thoracic Aortic Aneurysms* The New England Journal of Medicine, 1994. **331** (26): p. 1729-1734.

[35] T.E. MacGillivray, T.G. Gleason, H.J. Patel et al. *The Society of Thoracic Surgeons/American Association for Thoracic Surgery Clinical Practice Guidelines on the Management of Type B Aortic Dissection* Ann. Thorac. Surg, 2021; XX-XX

[36] Lombardi, J.V., G.C. Hughes, J.J. Appoo, J.E. Bavaria, A.W. Beck et. al. *Society for Vascular Surgery (SVS) and Society of Thoracic Surgeons (STS) Reporting Standards for Type B Aortic Dissections* J. Vasc. Surg., 2020. **71**: p. 723-47.

[37] D. Fleischmann et. al. *Imaging and Surveillance of Chronic Aortic Dissection: A Scientific Statement from the American Heart Association* Circulation Cardiovascular Imaging, 2022. **15**: e000075.

[38] Jan. J. Koenderink *Solid Shape* The MIT Press, Cambridge, Massachustts, 1990.

[39] D'Arcy Thompson *On Growth And Form* Dover, 1917.

[40] Tristan Needham *Visual Differential Geometry and Forms - a mathematical drama in five acts* Princeton University Press, Princeton, NJ, 2021.

[41] Barrett O'Neill *Elementary Differential Geometry, 2nd ed* Academic Press, Burlington, MA, 2006.

[42] Hilbert *Geometry and the Imagination* American Mathematical Society

[43] Michael Spivak *A Comprehensive Introduction to Differential Geometry, Volume 2, 3rd ed.* Publish or Perish, Inc., Huston, TX, 1999: pp. 147-150.

[44] Lo, S.H. and T.S. Lau. *Mesh generation over curved surfaces with explicit control on discretization error.* Engineering Computations, 1998. **15** (3), pp. 357-373.

[45] Z. Pennec, S. Sommer, and T. Fletcher *Riemannian Geometric Statistics in Medical Image Analysis.* Academic Press, Burlington, MA, 2020.

[46] Dacu, S., S. Haesen, adn L. Verstraelen. *Optimal Inequalities Characterizing Quasi-Umbilical Submanifolds.* J. Inequal. Pure and Appl. Math, 2008. **9** (3), p7

[47] Aguilar Gutierrez, O.F. and A.D. Rey. *Extracting Shape from Curvature Evolution in Moving Surfaces.* Soft Matter, 2018. **14**, 1465.

[48] McClure, J.E., S. Berg, and R.T. Armstrong. *Geometric Evolution as a Source of Discontinuous Behavior in Soft Condensed Matter.* arCIV:1906:04073v1, 2019

[49] Koenderink, J., van Doorn, A., and Wagemans, J. *Local Solid Shape.* i-Perception, 2015. **6** (5), 1-15.

[50] S. Rusinkiewicz *Estimating Cruvatures and Their Derivatives on Triangle Meshes.* Princeton University.

[51] Fillinger MF, Raghavan ML, Marra SP, Cronenwett JL, Kennedy FE. *In vivo analysis of mechanical wall stress and abdominal aortic aneurysm rupture risk.* J Vasc Surg. 2002;36(3):589-597. doi:10.1067/mva.2002.125478

[52] Sacks MS, Vorp DA, Raghavan ML, Federle MP, Webster MW. *In Vivo Three-Dimensional Surface Geometry of Abdominal Aortic Aneurysms.* Ann Biomed Eng. 1999;27(4):469-479. doi:10.1114/1.202

[53] Martufi G, Di Martino ES, Amon CH, Muluk SC, Finol EA. *Three-Dimensional Geometrical Characterization of Abdominal Aortic Aneurysms: Image-Based Wall Thickness Distribution.* J Biomech Eng. 2009;131(6):061015. doi:10.1115/1.3127256

[54] Shum J, Xu A, Chatnuntawech I, Finol EA. *A Framework for the Automatic Generation of Surface Topologies for Abdominal Aortic Aneurysm Models.* Ann Biomed Eng. 2011;39(1):249-259. doi:10.1007/s10439-010-0165-5

[55] Lee K, Zhu J, Shum J, et al. *Surface Curvature as a Classifier of Abdominal Aortic Aneurysms: A Comparative Analysis.* Ann Biomed Eng. 2013;41(3):562-576. doi:10.1007/s10439-012-0691-4

[56] Muluk SL, Muluk PD, Shum J, Finol EA. *On the Use of Geometric Modeling to Predict Aortic Aneurysm Rupture.* Ann Vasc Surg. 2017;44:190-196. doi:10.1016/j.avsg.2017.05.014

[57] de Galarreta SR, Cazon A, Anton R, Finol EA. *The Relationship Between Surface Curvature and Abdominal Aortic Aneurysm Wall Stress.* J Biomech Eng. 2017;139(8). doi:10.1115/1.4036826

[58] Chauhan SS, Gutierrez CA, Thirugnanasambandam M, et al. *The Association Between Geometry and Wall Stress in Emergently Repaired Abdominal Aortic Aneurysms.* Ann Biomed Eng. 2017;45(8):1908-1916. doi:10.1007/s10439-017-1837-1

[59] Urrutia J, Roy A, Raut SS, Antón R, Muluk SC, Finol EA. *Geometric surrogates of abdominal aortic aneurysm wall mechanics.* Med Eng Phys. 2018;59:43-49. doi:10.1016/j.medengphy.2018.06.007

[60] Tang A, Kauffmann C, Tremblay-Paquet S, et al. *Morphologic evaluation of ruptured and symptomatic abdominal aortic aneurysm by three-dimensional modeling.* J Vasc Surg. 2014;59(4):894-902.e3. doi:10.1016/j.jvs.2013.10.097

[61] Ma B, Harbaugh RE, Raghavan ML. *Three-Dimensional Geometrical Characterization of Cerebral Aneurysms.* Ann Biomed Eng. 2004;32(2):264-273. doi:10.1023/B:ABME.0000012746.31343.92

[62] Circulatory System Devices Panel *Real World Surveillance of AAA Endovascular Stent Grafts.* FDA Executive Summary, November 3rd, 2021.

[63] Liang L, M. Liu, C. Martin, J.A. Elefteriades, and W. Sun. *A Machine Learning Approach to Investigate the Relationship Between Shape Features and Numerically Predicted Risk of Ascending Aortic Aneurysm.* Biomech Model Mechaniobiol 2017; (16):1519-1533. doi 10.1007/s10237-017-0903-9.

[64] Casciaro, ME, D. Craiem, G. Chironi, S. Graf, L. Macron, E. Mousseaux, A. Simon, and R.L. Armentano. *Identifying the Principal Modes of Variation in Human Thoracic Aorta Morphology.* J. Thorac Imaging. 2014; (29):224-232.

[65] Grigory Isaakovich Barenblatt *Scaling, Self-Similarity, and Intermediate Asymptotics: Dimensional Analysis and Intermediate Asymptotics - Cambridge Texts in Applied Mathematics, Series 14* Cambridge University Press, Cambridge, UK. 1996.

[66] R. Thom. *Topological Models in Biology.* Topology. 1969; (8):313-335.

[67] Giannoglou, G, G. Giannakoulas, J. Soulis, Y. Chatzizisis, T. Perdikides, N. Melas, G. Parcharidis, and G. Louridas. *Predicting the Risk of Rupture of Abdominal Aortic Aneurysms by Utilizing Various Geometrical Parameters: Revisiting the Diameter Criterion.* Angiology. 2006;57(4):487-494. doi:10.1177/0003319706290741

[68] Lo, R., Bensley, R., Hamdan, A., Wyers, M., Adams, J. and Schermerhorn, M. *Gender differences in abdominal aortic aneurysm presentation, repair, and mortality in the Vascular Study Group of New England.* Journal of Vascular Surgery. 2013; 57(5):1261-1268.e5.

[69] Mehta, M., Byrne, W., Robinson, H., Roddy, S., Paty, P., Kreienberg, P., Feustel, P. and Darling, R. *Women derive less benefit from elective endovascular aneurysm repair than men.* Journal of Vascular Surgery. 2012; 55(4): 906-913.

[70] Compared to pure cylinders and tori of different size, the aortas are slightly more positive with a greater positive deviation for more disease states. This is an indication of some degree of excess positive curvature creation that is not balanced by exactly by negative curvature.